Schemel Award Paper

Evrard Lacroix,[1] Pierre-Clément A. Simon,[2]
Arthur T. Motta,[2] and Jonathan D. Almer[3]

Zirconium Hydride Precipitation and Dissolution Kinetics in Zirconium Alloys

Citation

E. Lacroix, P.-C. A. Simon, A. T. Motta, and J. D. Almer, "Zirconium Hydride Precipitation and Dissolution Kinetics in Zirconium Alloys," in *Zirconium in the Nuclear Industry: 19th International Symposium*, ed. A. T. Motta and S. K. Yagnik (West Conshohocken, PA: ASTM International, 2021), 67–91. http://doi.org/10.1520/STP162220190035[4]

ABSTRACT

Hydride precipitation may impact the integrity of zirconium-based nuclear fuel cladding, both during normal operation and during extended dry storage. To better understand such degradation, a study of hydride precipitation of zirconium hydrides in Zircaloy-4 samples was performed. The samples were submitted to various thermomechanical cycles using both in situ synchrotron X-ray diffraction and differential scanning calorimetry. Results showed that as the hydrided samples were cooled at moderate to fast cooling rates, the hydrogen content in solid solution (C_{SS}) decreased, following the terminal solid solubility for precipitation (TSS_P) curve, reflecting hydride precipitation in the matrix. However, when the samples were held for an isothermal anneal at a fixed temperature, the C_{SS} continued to decrease below TSS_P and approached the terminal solid solubility for dissolution (TSS_D). This result suggests that TSS_P is a kinetic limit and that a unique solubility limit TSS_D governs zirconium hydride precipitation. Hydride precipitation rate and the degree of precipitation reaction

[1]Framatome Inc., 3315 Old Forest Rd., Lynchburg, VA 24504, USA http://orcid.org/0000-0003-2592-2303

[2]The Pennsylvania State University, Dept. of Nuclear Engineering, 233 Hallowell Building, University Park, PA 16802, USA P.-C. A. S. http://orcid.org/0000-0001-7083-2628, A. T. M. http://orcid.org/0000-0001-5735-1491

[3]Advanced Photon Source, Argonne National Laboratory, Argonne, IL 60439, USA http://orcid.org/0000-0002-1900-2271

completion between 280 and 350°C were obtained using differential scanning calorimetry. Using this data, a temperature-time transformation diagram for hydride precipitation in Zircaloy-4 was generated that showed that hydride precipitation is diffusion-driven under 310°C and reaction-driven above 310°C. The experimental data were fitted to the Johnson-Mehl-Avrami-Kolmogorov model and an Avrami parameter of 2.56 was obtained (2.5 is the theoretical value for the growth of platelets). Results imply that hydride nucleation occurs if C_{SS} is greater than TSS_P while hydride growth occurs if preexisting hydride platelets are present and C_{SS} is above TSS_D. Combined with existing theory, these data were used to develop the hydride growth, nucleation, and dissolution model that can simulate hydrogen behavior in Zircaloy.

Keywords

zirconium, zirconium hydride, nuclear, precipitation, dissolution, hydride nucleation, hydride growth, modeling

Introduction

BACKGROUND

Nuclear fuel cladding undergoes corrosion under normal operating conditions of nuclear power reactors. During that process, the zirconium (Zr) of the cladding reacts with water to form zirconium oxide. A fraction of the hydrogen produced during the waterside corrosion is picked up by the cladding.[1–3]

When the hydrogen concentration in the cladding reaches the solubility limit, brittle zirconium hydride (ZrH_x) particles precipitate.[1,4–6] The most commonly observed hydride phase is the face-centered cubic δ-hydride, with a lattice parameter of 4.37 Å and $x \approx 1.66$.[6]

To assess cladding integrity, it is important to be able to quantitatively predict the precipitation of brittle hydrides. It is therefore essential to obtain a reliable description of the hydrogen solubility in Zircaloy[4–9] and to understand the precipitation mechanisms.[10–14] Current hydride precipitation models are not mechanistic in that when simulating hydride precipitation, no differentiation between hydride nucleation and hydride growth is made, whereas the two precipitation mechanisms occur under different conditions and are governed by different time constants. This can lead to inaccuracies in the prediction of hydrogen precipitation and its distribution in the cladding. A comprehensive hydrogen precipitation and dissolution model is proposed here. A series of experiments was performed to differentiate hydride growth from hydride nucleation, and the precipitation kinetics of each mechanism was studied to derive a comprehensive model.

HYDRIDE PRECIPITATION

Previous studies have shown that, under the right conditions, hydrides can precipitate between terminal solid solubility for precipitation (TSS_P) and terminal solid solubility for dissolution (TSS_D)[6,15] (i.e., when a sample is heated without dissolving all the

hydrides and then cooled, hydride precipitation occurs as soon as cooling starts).[6] This is contrary to the belief that hydrides precipitate only if the hydrogen content in solid solution is greater than the TSS_P for that temperature.[4,5,10,13] With this result in mind, an experiment was previously performed to characterize hydride precipitation behavior in the hysteresis region (between TSS_P and TSS_D) of the zirconium-zirconium hydride system.[15] Three notable results were obtained: (i) hydride precipitation occurs immediately upon cooling if hydride particles are not completely dissolved during heating, (ii) during an isothermal hold, zirconium hydride precipitation continued even when the hydrogen content in solid solution was below TSS_P, and (iii) precipitation during a temperature increase was observed as long as the concentration of hydrogen in solid solution was above TSS_D.[15]

Continuous in situ cooling experiments using the synchrotron prove to be an effective way to measure the different terminal solid solubilities.[6,16] The hydrogen solubilities (TSS_D and TSS_P) obtained using differential scanning calorimetry (DSC)[4] and using in situ synchrotron radiation diffraction[16] match almost exactly. Because the DSC technique measures the *nucleation* temperature,[4] this agreement suggests that the TSS_P corresponds to the maximum amount of hydrogen in solid solution that the matrix can accommodate before hydride nucleation occurs. This nucleation limit is typically called the *supersolubility* limit.[17] Note that the hydrogen content in solid solution can exceed the typical value observed for TSS_P if the cooling rate is high enough[16] that hydride nucleation cannot compensate for the high rate of change in the TSS_P as the temperature decreases.

In summary, two processes occur during hydride precipitation: a fast nucleation process that is typically observed during continuous cooling and a slow process observed during long isothermal holds and that is related to hydride growth. In this study, this understanding is used to propose a revised model of hydride precipitation and dissolution.

EXPERIMENTAL METHODS

The experiments were performed using cold-worked stress-relieved Zircaloy-4 sheets (0.7 mm thick) provided by ATI Specialty Alloys and Components. Chemical analysis of oxygen and hydrogen performed by Luvak, Inc., on the as-received samples showed that the starting material contained 16 ± 1 wt. ppm of hydrogen and $1,122 \pm 50$ wt. ppm of oxygen. The material texture was such that the basal poles were inclined approximately $\pm 30°$ away from the normal direction of the sheet.[18,19] The measured Kearns factors of the sheet material[20] were: $f_N = 0.59$, $f_L = 0.05$, and $f_T = 0.31$ in the normal, longitudinal, and transverse directions, respectively. These values are similar to those normally obtained in cold-worked stress-relieved Zircaloy-4 cladding.[21]

The samples were cut from sheet material into rectangular samples 2 cm by 5 cm and etched using a solution containing 10% vol. hydrofluoric acid (49% concentrated), 45% vol. nitric acid (89% concentrated), and 45% vol. deionized water until the sample surface showed a mirror finish. A 20-nm nickel layer was then deposited on the sample to protect it from air oxidation while allowing hydrogen

ingress. The material was hydrided by gaseous charging: a mixture of hydrogen and argon gas was introduced in a vacuum chamber where the samples were heated to 450°C. Samples A and B were then machined using wire electrical discharge machining into dog-bone samples approximately 660 μm thick. The exact dog-bone dimensions are shown in **figure 1** of Lacroix, Motta, and Almer.[15] The material removed from the machining process was sent to Luvak, Inc., for hydrogen testing using vacuum hot extraction (in accordance with ASTM E146, *Methods of Chemical Analysis of Zirconium and Zirconium Alloys* [*Silicon, Hydrogen, and Copper*]). The hydrogen content of the different samples was measured and found to be 165 ± 12 wt. ppm in Sample A, 166 ± 13 wt. ppm in Sample B, 183 ± 31 wt. ppm in Sample C, and 264 ± 20 wt. ppm in Sample D.

Samples A and B, having the same hydrogen content, were examined at the Advanced Photon Source (APS) at Argonne National Laboratory (beamline 1-ID-E) to study the effect of applied stress in the transverse direction on hydride precipitation and dissolution. Samples C and D were used to determine hydride growth kinetics at constant temperatures using differential scanning calorimetry at Penn State University. Brief descriptions of the experimental techniques and experiments performed are given here.

DSC Experiments

Isothermal precipitation experiments were performed on Samples C and D following ASTM E2070-13, *Standard Test Method for Kinetic Parameters by Differential Scanning Calorimetry Using Isothermal Methods*.[22] Sample C (183 wt.ppm) was cut into five different samples weighing between 4 mg and 7 mg, thus allowing testing

FIG. 1 Temperature history and heat flow evolution when measuring hydride precipitation at 301°C for Sample C, using DSC. The heat flow required to hold the sample at a constant temperature provides information about the hydride precipitation reaction.
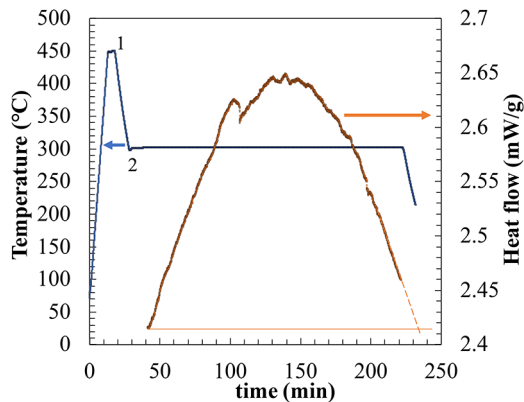
of the isothermal hydride precipitation in sister samples (with the same hydrogen content) at five different temperatures, while a 6-mg sample of Sample D (264 wt.ppm) was used. The sister samples from Sample C were heated up to 420°C at a rate of 20°C/min, while Sample D was heated to 450°C at a rate of 15°C/min. In both cases, samples were held at the highest temperature for 10 min to dissolve all the hydrides and homogenize the hydrogen in solid solution. Samples were then cooled down to a fixed temperature and held at that temperature for 4 to 5 h to allow the hydride precipitation reaction to approach completion. The evolution of the reaction can be observed through the heat released by the exothermic reaction between the hydrogen in solid solution and the zirconium to form hydrides. An example of this evolution can be seen in figure 1. At the beginning, a high driving force exists for hydride growth but with a low volume fraction of hydrides. As the reaction progresses, the driving force diminishes but the hydride volume fraction increases. This evolution is mirrored by the curve obtained, where the maximum of the curve corresponds to an optimal driving force and volume fraction of hydrides for hydride growth. After the temperature hold, the samples were cooled to room temperature. In this study, the temperatures tested for isothermal growth were 280, 290, 301, 305, 320, and 350°C. Sample D was used to perform the test at 350°C as Sample C contained an insufficient amount of hydrogen for precipitation to occur at that temperature. The results obtained were used to create a temperature-time transformation (TTT) diagram for isothermal hydride precipitation.

Synchrotron Radiation Diffraction Experiments

High-energy synchrotron radiation diffraction has been used to study hydride precipitation and dissolution in zirconium alloys.[6,9,11,15,16,23,24] Using high-energy X rays, it is possible to acquire data on both the hydride and zirconium matrix diffraction and to obtain a direct measurement of the precipitation and dissolution behavior of hydrides in situ, that is, at temperature and under stress.[6,11,16,24,25]

The experiments described as follows were performed at the APS using a 300 by 300 μm monochromatic beam of 71.676 keV, calibrated with a cerium oxide standard. The data were then obtained by summing 25 diffraction patterns taken for 0.1 s each to provide good signal-to-noise ratio while avoiding detector saturation. Every summed diffraction pattern was analyzed using the same MATLAB script as used in previous work.[15] Figure 2 shows the heat treatment applied to Sample A (blue) along with the integrated peak intensity of the $\delta(111)$ hydride diffraction peak (orange). The integrated peak intensity was compared at the beginning and the end of each heat treatment to make sure no hydrogen was lost during the experiment. In addition, a linear scan was performed prior to the beginning of each experiment to verify the homogeneous distribution of hydrogen within ± 5mm of the beam. No significant diffusion of hydrogen is therefore expected to have occurred during the experiment (the diffusion distance at 400°C for hydrogen is smaller than 5 mm for the duration of the experiments). The hydrogen content of each sample was also tested by vacuum hot extraction on two opposite sides of the

FIG. 2 Heat treatment applied to Samples A and B during examination at Argonne National Laboratory's Advanced Photon Source (solid line) and integrated δ(111) integrated peak intensity signal (markers) at each measurement time.
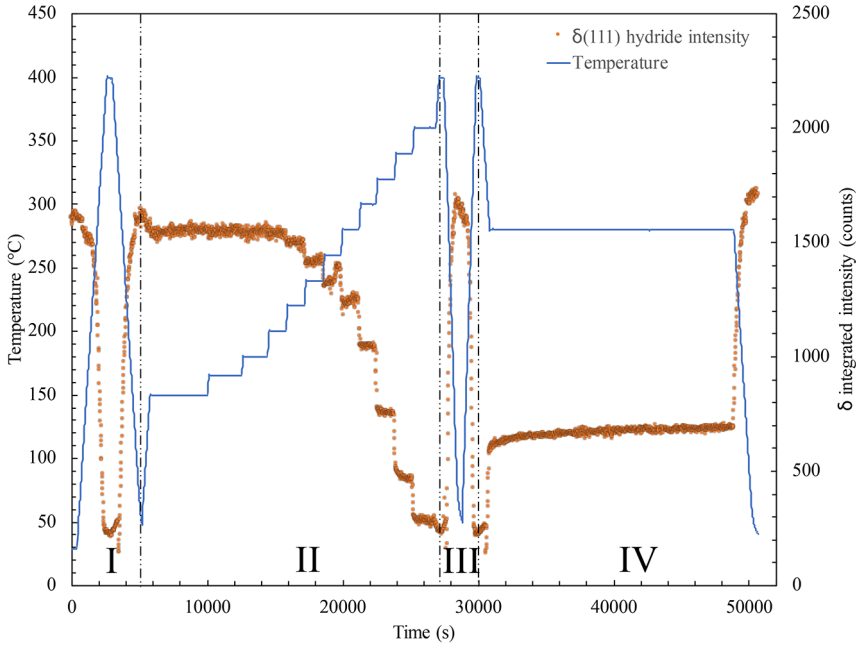
area exposed by the beam and showed no more than 10 ppm of deviation. The heat treatment can be subdivided into four experiments, referred to as I, II, III, and IV in figure 2. The same heat treatment was applied to Sample B. Different uniaxial tensile stresses were applied to the two samples during their heat treatment (0 and 200 MPa, respectively) to study the influence of applied stress on hydride nucleation, growth, and dissolution. The applied stress level was enough to cause hydride reorientation.[24] The experiments are:

- Experiment I: Effect of Stress on TSS_P

Two samples with the same hydrogen concentration (Samples A and B) were heated to a temperature high enough for hydride dissolution, then cooled to observe hydride precipitation. During the experiment, no stress was applied to Sample A and a tensile stress of 200 MPa was applied to Sample B. The hydrogen content in solid solution in the sample was estimated using the integrated diffracted intensity of the δ(111) hydride peak.

- Experiment II: Effect of Heating Rate and Stress on TSS_D

In this experiment, a well-measured TSS_D curve was obtained by stepwise heating a sample and allowing equilibrium to be established at each point. The hold times

were established by taking the higher of 20 min or the typical diffusion time $t = l^2/D(T)$ where l is the diffusion distance and D is the hydrogen diffusion coefficient. The diffusion distance is defined as half the distance between two macro hydrides in the material; $l = 100$ μm was chosen as a conservative estimate.

- Experiment III: Effect of Stress on Nucleation and Dissolution Kinetics

As shown previously, when the rate of temperature change is about 20°C/min or higher, the hydrogen content in solid solution deviates from the TSS_D (during heating) and from the TSS_P (during cooling).[16] Although it has been suggested that this is caused by the greater difficulty of hydrides to nucleate at high cooling rates,[16] this study hypothesizes that this deviation is caused by the δ-hydride dissolution kinetics (during heating) and the δ-hydride nucleation kinetics (during cooling) becoming rate-limiting. To test this hypothesis, the samples were heated and cooled at 20°C/min to measure the δ-hydride dissolution kinetics and δ-hydride nucleation kinetics under no stress and under an applied 200 MPa tensile stress and to observe any effects of applied stress on hydride nucleation and dissolution.

- Experiment IV: Hydride Precipitation during Isothermal Hold

The two samples (A and B, with 0 and 200 MPa applied stress, respectively) were cooled from 400°C (end of Experiment III) to 280°C at a rate of 10°C/min. The samples were then held at that temperature for 5 h to measure the hydride growth kinetics and then cooled to room temperature at a rate of 10°C/min. The results of these experiments are discussed in the following section.

Experimental Results

ISOTHERMAL GROWTH MEASURED USING DSC

In this section, the results obtained during isothermal precipitation of zirconium hydrides using ASTM E2070-13[22] are discussed. The standard recommends using the Johnson-Mehl-Avrami-Kolmogorov (JMAK) model[26–28] for crystallization reactions. In the JMAK model, the precipitation reaction is described by equation (1):

$$X(t) = 1 - \exp(-(K_G \cdot t)^p) \tag{1}$$

where t is the time; K_G is the growth kinetics parameter, following an Arrhenius law specific to the reaction; p is the Avrami parameter; and $X(t)$ is the advancement of the reaction at the time t defined by equation (2):

$$X(t) = \frac{C_{PP(t)}}{C_0 - TSS_D} \tag{2}$$

where C_{PP} is the hydrogen content in hydride form, and C_0 is the total hydrogen content in the sample (all in wt.ppm). When all the hydrogen content above TSS_D is in the form of hydrides, then $X = 1$. The advancement of the reaction $X(t)$ at a given time is obtained by first integrating the heat flow in figure 1 from the start of the isothermal reaction to the time t, using equation (3):

$$\Delta H_r(t) = \int_0^t q(t')dt' \tag{3}$$

where $q(t')$ is the heat flow measured by DSC at the time $t' < t$. If the TSS_P and TSS_D values are known at the temperature of interest, $X(t)$ can be obtained using equation (2) and is shown as equation (4):

$$X(t) = \frac{C_0 - TSS_P + \dfrac{\Delta H_r(t)}{\Delta H_r(t = t_{end})} \cdot (TSS_P - TSS_D)}{C_0 - TSS_D} \qquad (4)$$

where t_{end} is the time at the end of the reaction. Once $X(t)$ is known, K_G and p can be obtained by plotting $ln(-ln[1 - X])$ versus $ln(t)$. Equation (5) then results from equation (1):

$$ln(-ln(1 - X)) = p \cdot ln(K_G) + p \cdot ln(t) \qquad (5)$$

Figure 3 shows a TTT plot for hydride precipitation in Zircaloy-4, as derived by DSC using the method described previously. The points represent experimental measurements while the curves represent calculations performed using the model

FIG. 3 Experimental TTT diagram from DSC data fitted for a sample with a hydrogen content of 205 wt.ppm (right) and 264 wt.ppm (left). The hydrogen content of 205 wt.ppm was chosen as the actual value from the precipitation temperatures obtained experimentally as this value falls within the uncertainty band and agrees with the TSS_P values from the literature. The data point at 264 wt.ppm was added to validate the extrapolation to higher hydrogen content. Simulations accounting for sample hydrogen content measurement uncertainties are provided (dashed lines). The simulated TTT diagrams range from 250°C to the precipitation temperature obtained from TSS_P measurements performed by Une and Ishimoto.[4]
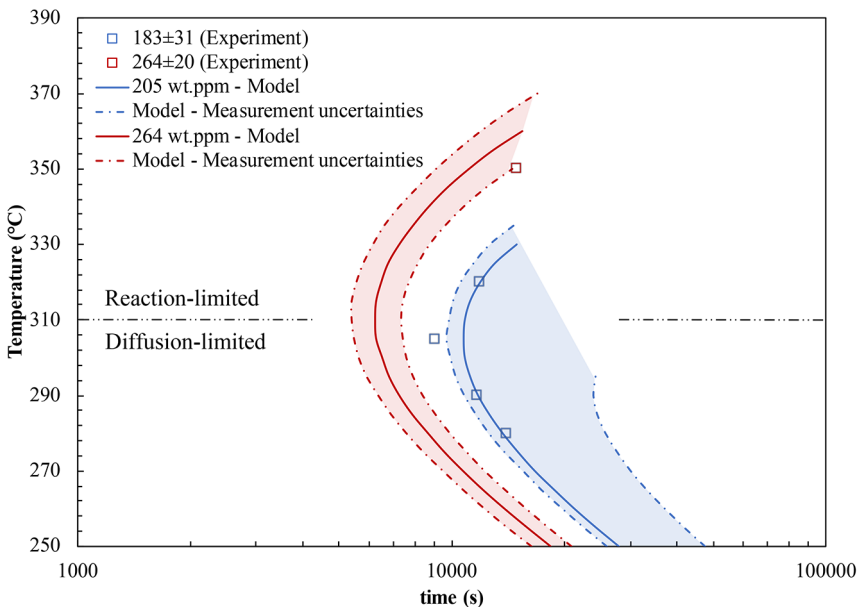
presented in this paper, for the two samples (C and D). The uncertainty bands shown in **figure 3** are obtained by inserting the uncertainties in hydrogen content into the reaction advancement calculation in equation (4). By repeating the experiment at different temperatures, it is possible to obtain the temperature dependence of K_G and obtain a TTT diagram of the precipitation reaction by plotting the test temperature as a function of the time necessary to reach a certain reaction stage; $X = 0.99$ was chosen to obtain the TTT diagram in **figure 3**.

The precipitation reaction rate is low at low temperature and increases with temperature, reaching a minimum completion time around 310°C for Sample C (containing 183 ± 31 wt.ppm of hydrogen), and then it slows down as temperature increases further. This behavior is typical of TTT diagrams and is usually explained as a diffusion-driven process at low temperature and a reaction-driven process at high temperature.

As mentioned, diffusion-limited growth occurs below 310°C, and the constant in equation (1) is $K_G = K_G^D$ under 310°C, expressed in s^{-1}. Thus, the experiments performed below 310°C were used to measure the diffusion-limited growth kinetics variable K_G^D; K_G^D was fitted using equation (5) and plotting $ln(-ln[1 - X])$ versus $ln(t)$ at different temperatures (280, 290, 301, and 305°C), assuming the reaction-limited growth kinetics component K_G^R has a negligible effect on the fit at these temperatures and that, therefore, $K_G \approx K_G^D$. **Figure 4** shows a plot of $ln(K_G)$ as a function of inverse temperature (K^{-1}), assuming $K_G = K_G^D$ follows an Arrhenius law. The uncertainties are obtained by performing the calculations assuming the outside bounds of the hydrogen content measurement for Sample C when calculating the

FIG. 4   Experimental values of the growth kinetic parameter assuming a diffusion driven process $K_G \approx K_G^D$ versus inverse temperature compared to different fits of K_G within the bounds of experiment errors. Experimental values are fitted to feed the model with an accurate value of the parameter K_G^D, which is crucial to predict the growth kinetics.
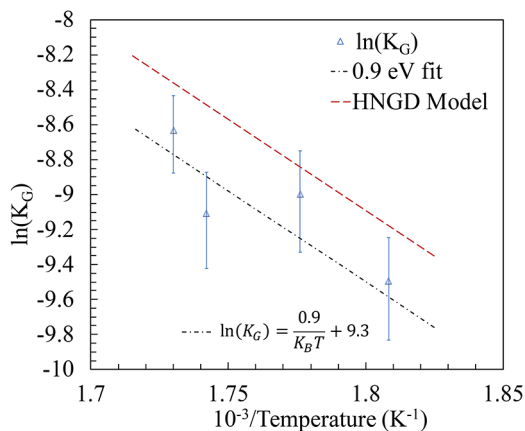
reaction advancement (equation [4]). While the Avrami parameter was found to be $p = 2.56 \pm 0.14$ (approximately corresponding to the growth of platelets with no nucleation, p = 2.5) the fit of K^D obtained implies an activation energy for growth by diffusion (E^G) of 0.9 eV/atom. This activation energy is higher than that expected for the diffusion process of hydrogen (0.44–0.47 eV/atom).[29,30] This discrepancy could arise from dislocations surrounding the hydrides, which interact with the hydrogen in solid solution and slow the diffusion of hydrogen toward the hydride. Note also that the pre-exponential factor of K^D was affected when incorporating it in the model to account for the contribution of the reaction-limited growth (the model value of K^D shown with the red dashed line in figure 4 is slightly greater than the value fitted with $E^G = 0.9$ eV/atom).

Not much data were obtained in the temperature range where the high-temperature reaction-driven process is dominant. As a result, it was not possible to fit the data in the same manner as was done in the diffusion-driven process temperature region. It will, however, be shown in the following section that the reaction-driven process can be simulated using the formation energy of the δ-hydride.

## ISOTHERMAL GROWTH MEASURED USING SYNCHROTRON X-RAY DIFFRACTION

Experiment IV was designed to study hydride growth. Samples A and B (165 wt.ppm) were cooled down from 400°C at a constant rate of 10°C/min until the hold temperature of 280°C was reached. This was done at zero stress for Sample A and 200 MPa for Sample B. The reaction only progressed by 10% during the 5-h isothermal reaction, contrary to what was observed by Courty et al.[11] Therefore, it was not possible to perform kinetic measurements. (The ASTM standard recommends performing measurements on advancements evolving from 30 to 70%.[22]) The fact that this reaction was slower than expected was possibly caused by a dependence of the kinetics reaction on hydrogen content or cooling rate. These factors can affect the surface density available for additional hydride growth and therefore change hydride growth kinetics (the higher the surface density, the more growth sites are available and the faster the growth kinetics will be).

Figure 5 shows the amount of hydrogen in solid solution increases with applied stress (the applied stress increases the TSS_P), indicating that the precipitation of reoriented hydrides occurs at a *lower temperature* than the precipitation of in-plane hydrides, as seen previously.[6] In contrast, no significant change in the hydride growth rate can be observed during the reaction observed as the curves are parallel.

INFLUENCE OF STRESS ON HYDROGEN SOLUBILITY

Experiments I and II were used to determine whether applied stress influences the terminal solid solubilities in the zirconium/zirconium hydride system. Experiment I was designed as a dynamic experiment to measure TSS_P, while Experiment II was designed to measure the equilibrium value of hydrogen in solid solution at different temperatures (TSS_D), thereby obtaining the influence of applied stress on both TSS_P and TSS_D.

FIG. 5   Hydrogen content in solid solution as a function of hold time at 280°C during
Experiment IV, for Sample A (0 MPa) and Sample B (200 MPa). The hydrogen
content is obtained from the (111) peak of the δ-zirconium hydride phase. The
precipitation kinetics do not seem to be affected by stress while TSS_P increases
with tensile stress.
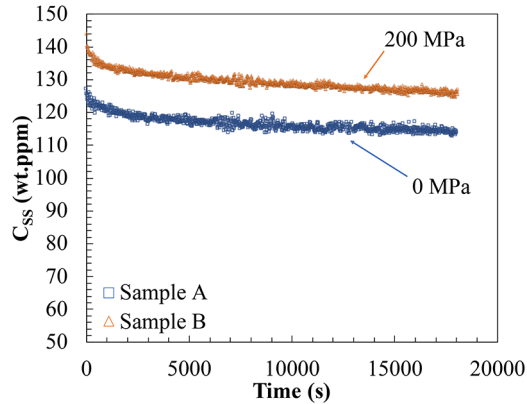
As shown in **figure 2**, in Experiment II, the temperature is increased by steps
and the hydride diffracted intensity is evaluated at each step. The calculated values
of C_{SS} obtained as in previously published work[15] are then taken as the TSS_D at that
temperature. **Figure 6** shows the logarithm of the equilibrium value of hydrogen in

FIG. 6   Terminal solid solubility for dissolution measured using synchrotron radiation
diffraction for Samples A and B, using the hydride diffraction peaks (111) and
(220) and at two different uniaxial applied stress conditions (0 MPa for Sample
A and 200 MPa for Sample B).
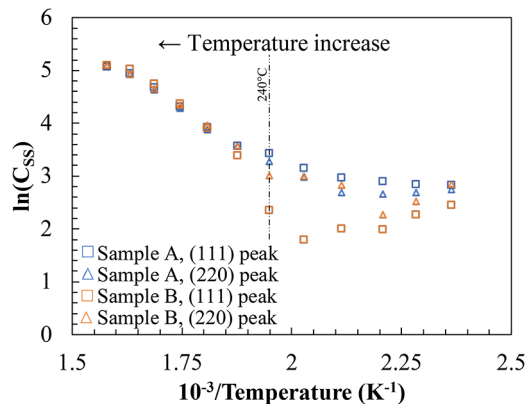
solid solution ($ln[C_{SS}]$) thus obtained versus inverse temperature using the (111) and (220) peak intensities with and without applied stress (Samples A and B). No significant difference is seen between the different values obtained above 240°C, indicating that the contribution of applied stress on TSS_D of hydrogen in zirconium alloys above 240°C, if any, is small. It is more challenging to discuss the results at lower temperatures as it is unclear if equilibrium was reached in the lower temperatures. However, note that the hydrogen content in solid solution derived from the (220) hydride integrated peak intensities is nearly the same between the samples under 0 and 200 MPa applied tensile stress, while the hydrogen in solid solution obtained from the (111) integrated peak intensity at 200 MPa is significantly lower from 150 to 260°C. This difference could arise from the specific hydride platelet orientation relative to the incident beam.

Thus, it can be said that while TSS_P is impacted by the applied stress, TSS_D is not significantly affected, at least not in the temperature range studied. The results indicate that greater undercooling is needed for precipitation of reoriented hydrides under an applied stress of 200 MPa than for in-plane hydrides precipitated under no stress. The fits of the TSS_D and TSS_P under different applied tensile stress are provided in equation (6). The TSS_P interpolations were derived from the δ(111) peak as it is more intense and allows a better fit, while results obtained are not affected, as described earlier and shown in figure 6.

$$
\begin{cases}
TSS_D = 2.05 \times 10^6 \cdot \exp\left(-\dfrac{48710}{RT}\right) \\[2mm]
TSS_P(0\,MPa) = 5.47 \times 10^4 \cdot \exp\left(-\dfrac{27855}{RT}\right) \\[2mm]
TSS_P(200\,MPa) = 1.13 \times 10^5 \cdot \exp\left(-\dfrac{30506}{RT}\right)
\end{cases}
\qquad (6)
$$

where R is the ideal gas constant (in J mol^{-1} K^{-1}), T is the temperature (in K), and the solubilities are given in wt.ppm.

HYDRIDE NUCLEATION KINETICS

When the hydrogen in solid solution reaches TSS_P, hydrides nucleate at a rate given by the nucleation kinetics. If the cooling rate is fast enough, the nucleation kinetics will limit the hydride precipitation rate. If not, the hydride precipitation rate will be dictated by the cooling rate. To study hydride nucleation kinetics, it is necessary to cool the sample at a fast enough rate that hydride precipitation is governed by nucleation kinetics rather than by the cooling rate. As mentioned previously, it has been shown that at cooling rates of 1 to 10°C/min, the measured TSS_P is little affected, but at higher cooling rates (greater or equal to 20°C/min), the TSS_P increases,[16] suggesting that for higher cooling rates, nucleation kinetics start to limit hydride precipitation. As a result, in Experiment III, a cooling rate of 20°C/min was used to cool Samples A and B from 400°C to 50°C, and the hydride nucleation kinetics were measured in each case. Precipitation above TSS_P has been previously

modeled by a first-order equation,[31] and thus it is hypothesized here that the nucle-ation kinetics follow this same law:

$$\frac{dC_{SS}}{dt}(t) = K_N(T) \cdot (C_{SS}(t) - TSS_P(T))$$ (7)

where K_N is the nucleation kinetics parameter, following an Arrhenius law (in s^{-1}). In order to measure the nucleation kinetics at each time step, equation (7) was writ-ten in finite difference form to obtain equation (8):

$$K_N(T(t + \Delta t)) = \frac{C_{SS}(t + \Delta t) - C_{SS}(t)}{\Delta t \left(C_{SS(t)} - TSS_P(T(t + \Delta t))\right)}$$ (8)

The kinetics parameter $K_N(T)$ was obtained using two consecutive hydride diffrac-tion intensity measurements from the synchrotron, at time t and $t + \Delta t$. At time t, the temperature is $T(t)$ and, therefore, $K_N = K_N(T[t])$ because the temperature changes with time.

The values used for $TSS_P(T)$ were those found in Experiment I interpolated for the temperatures studied in Experiment III. Figure 7 shows a plot of $ln(K_N)$ versus $1/T$ (in K^{-1}) for both the stressed and unstressed samples. The activation energy for the nucleation process can be calculated from the slope.

The hydride nucleation kinetics are almost identical for the samples cooled with and without applied stress. This suggests that the applied stress affects only the TSS_P and not the nucleation mechanism itself. The result of the fit obtained is shown in figure 7 and has a large associated uncertainty, most likely coming from a combination of high nucleation rates, long acquisition times (compared to the

---

FIG. 7 Plot of the logarithm of the nucleation kinetics constant K_N as a function of inverse temperature compared to the value used in the model presented in this study. The value used in the model falls within the uncertainty limits.
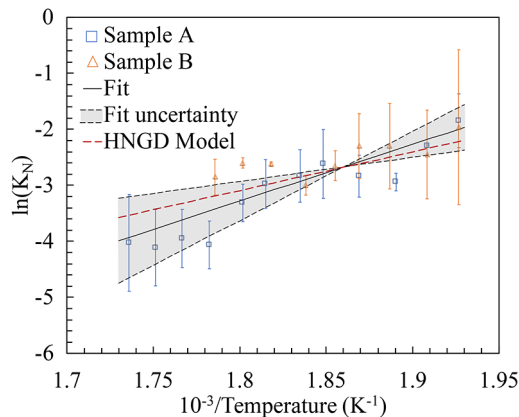
nucleation kinetics), peak fitting uncertainties, and uncertainties on the value of TSS_P at each time step. Nevertheless, ab initio calculations of hydride formation energies[32] fall within the activation energies measured here (between 0.4 and 1.4 eV/atom). The results obtained with the nucleation model for K_N, using an Arrhenius law based on different formation energies, are shown in figure 7 and agree with the experimental measurements. The model used in fitting the results shown in figure 7 is developed in the last section of this paper.

ZIRCONIUM HYDRIDE DISSOLUTION

As temperature increases, the solubility of hydrogen into zirconium increases; therefore, hydrides will dissolve. If the heating rate is slow enough, the dissolution of hydrides is fast enough to keep the system in quasi-equilibrium. The dissolution of hydrides is therefore linked to the sample heating rate. As the heating rate increases, the dissolution kinetics become the limiting step. As mentioned in the description of Experiment III, the sample heating rate is fast enough that the hydride dissolution rate is governed by the dissolution kinetics rather than by the heating rate. Previous work showed that TSS_D starts to change significantly for heating rates of 20°C/min or higher,[16] so the dissolution kinetics experiment was performed at that heating rate. The dissolution kinetics are also assumed to follow first-order kinetics, as proposed in previous work by Courty, Motta, and Hales.[10]

$$\frac{dC_{SS}}{dt}(t) = -K_D(T) \cdot (C_{SS}(t) - TSS_D(T)) \tag{9}$$

where K_D is the dissolution kinetics parameter (in s^{-1}) and is assumed to follow an Arrhenius law. The value of K_D was also obtained from two consecutive measurements of hydrogen content as the temperature increases. Equation 10 is obtained by rearranging the finite difference version of equation (8) into equation (9):

$$K_D(T(t + \Delta t)) = -\frac{C_{SS}(t + \Delta t) - C_{SS}(t)}{\Delta t \big(C_{SS(t)} - TSS_D(T(t + \Delta t)) \big)} \tag{10}$$

Data analysis showed that K_D did not vary monotonically with temperature. Therefore, it was decided to plot the evolution of the dissolution reaction (dependent on K_D) as a function of temperature similar to how TTT diagrams are plotted (i.e., by plotting the temperature as a function of time needed to achieve a given completion state of the transformation reaction). The completion state of 95% was chosen by taking $\tau = {}^1/{K_D}$ as the time constant of the process and plotting temperature as a function of 3τ. Figure 8 plots the temperature versus the time necessary to reach 95% of the hydride dissolution reaction and was obtained from measurements performed in unstressed (0 MPa) and stressed (200 MPa) samples. The prediction of the hydride growth, nucleation, and dissolution (HNGD) diffusion-based dissolution model described here is also shown as the red dotted line. The dissolution kinetics data in figure 8 show no significant influence of stress on the dissolution kinetics.

FIG. 8   Comparison of the value of $\tau = 3/K_D$ measured experimentally from Samples A (0 MPa) and B (200 MPa) and simulated (0 MPa) for the same heat treatment.
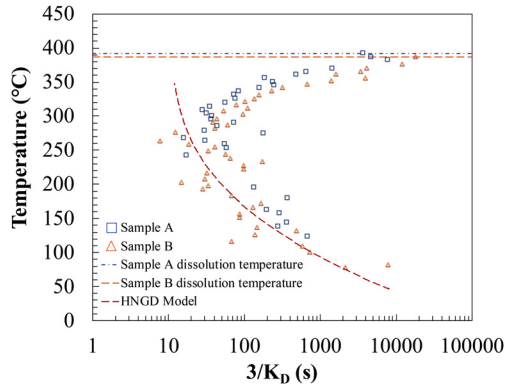
In the case of hydrides in zirconium alloys, hydride dissolution is likely limited by how fast hydrogen can diffuse away from the hydride once it is in solid solution so that further hydride dissolution can occur.[33] K_D was therefore assumed to follow an Arrhenius law, as shown in equation (11):

$$K_D(T) = K_D^0 \cdot \exp\left(-\frac{E_D}{k_B T}\right) \qquad (11)$$

where E_D is the activation energy for hydrogen diffusion in zirconium taken as $E_D = 0.46$ eV/atom.[30] However, the hypothesis that the dissolution is a diffusion-driven process appears to be limited to low temperatures in figure 8. While, as expected, the hydride dissolution kinetics parameter K_D consistently increases from 50 to about 300°C, the trend reverses above 320°C, and K_D seems to decrease until complete dissolution occurs at 390°C. The model predicts the dissolution kinetics well at low temperatures but not at high temperatures, suggesting a competition between a diffusion-driven mechanism at low temperatures and another mechanism at higher temperatures that has yet to be identified. The high temperature discrepancy in dissolution kinetics suggests further study is needed.

HNGD: A Comprehensive Hydride Precipitation and Dissolution Model

The previous sections described how the various precipitation and dissolution kinetics parameters were measured and what results were obtained. This section proposes a hydrogen model that incorporates the experimental work reported in the previous sections into a model referred to as the HNGD model. This section presents preliminary results of benchmark calculations.

EQUATIONS AND PARAMETERS

The Model

As proposed in a previous model,[10] the HNGD model is based on four different conditions in the system for hydrogen behavior. These conditions, shown in **table 1**, depend both on the hydrogen content in solid solution compared to the TSS_D and TSS_P values and the hydride content in the sample (referred to as C_{PP} in **table 1**). Each case represents a physical mechanism that corresponds to hydride nucleation, growth, or dissolution, as specified in **table 1**. Note that nucleation and growth can happen simultaneously.

The Parameters

As shown in **table 1**, four parameters are included in the model (K_N, K_G, p, and K_D) that control the hydride precipitation and dissolution reactions. The following details the values of these parameters as used in the model.

Nucleation: The parameter K_N is hypothesized to depend linearly on the volume fraction of the zirconium matrix f_α, reflecting work performed previously,[13] as shown in **equation (12)**:

$$K_N(t) = 2.75 \times 10^{-5} \cdot f_\alpha \cdot \exp\left(-\frac{\Delta E^a_{\alpha \to \delta}}{k_B T}\right) \quad [s^{-1}] \tag{12}$$

where $f_\alpha = 1 - \frac{x_{PP}}{x_\delta - x_\alpha}$, x_{PP} is the atomic fraction of hydrogen in the hydride form, x_δ is the atomic fraction of hydrogen content in a pure δ-hydride, x_α is the maximum atomic fraction of hydrogen in the α-zirconium phase, and $\Delta E^a_{\alpha \to \delta}$ is the activation energy for the nucleation of δ-hydrides from hydrogen in solid solution in α-zirconium. In this model, the activation energy is assumed to be

TABLE 1 HNGD model equations for the different system conditions

Conditions	Equations
Hydride nucleation $C_{SS} > TSS_P$	$\dfrac{dC_{PP}}{dt} = K_N \cdot (C_{SS} - TSS_P)$ $\dfrac{dC_{SS}}{dt} = -\dfrac{dC_{PP}}{dt}$
Hydride growth $C_{SS} > TSS_D \ \& \ C_{PP} > 0$	$\dfrac{dX}{dt} = K_G \cdot p \cdot (1 - X)(-\ln(1 - X))^{1 - \frac{1}{p}}$ $X = \dfrac{C_{PP}}{C_0 - TSS_D}, \dfrac{dC_{SS}}{dt} = -\dfrac{dC_{PP}}{dt}$
Hydride dissolution $C_{SS} \leq TSS_D \ \& \ C_{PP} > 0$	$\dfrac{dC_{PP}}{dt} = K_D \cdot (C_{SS} - TSS_D)$ $\dfrac{dC_{SS}}{dt} = -\dfrac{dC_{PP}}{dt}$
Phase equilibrium $C_{SS} < TSS_P \ \& \ C_{PP} = 0$ or $C_{SS} = TSS_D$	$\dfrac{dC_{SS}}{dt} = -\dfrac{dC_{PP}}{dt} = 0$

equal to the formation energy of the δ-hydride phase, $\Delta E^f_{\alpha \to \delta}$, which, as shown in figure 7, provides consistent results with the data gathered at the synchrotron; $\Delta E^f_{\alpha \to \delta}$ can be derived from the CALPHAD free energies G_α and G_δ of the α-Zr/δ-ZrH$_x$ system developed by Dupin et al.[34] and used by Jokisaari and Thornton.[35] Solving the system, as shown in equation (13):

$$\begin{cases} \dfrac{\partial G_\alpha}{\partial x}\left(x^{eq}_\alpha, T\right) = \dfrac{\partial G_\delta}{\partial x}\left(x^{eq}_\delta, T\right) \\ \dfrac{\partial G_\delta}{\partial x}\left(x^{eq}_\alpha, T\right) \times \left(x^{eq}_\delta - x^{eq}_\alpha\right) = G_\delta\left(x^{eq}_\delta, T\right) - G_\alpha\left(x^{eq}_\alpha, T\right) \end{cases} \quad (13)$$

where T is the temperature and provides both x^{eq}_α and x^{eq}_δ, which are the equilibrium concentrations of hydrogen in α-Zr and δ-ZrH$_x$, respectively. The formation energy is then derived as $\Delta E^{f(T)}_{\alpha \to \delta} = G^\delta(x^\delta_{eq}, T) - G^\alpha(x^\alpha_{eq}, T)$ for each temperature. A reasonable fit provides the following equation for the formation energy $\left(\Delta E^f_{\alpha \to \delta}\right)$ in eV/atom as a function of the temperature T (in Kelvin) in the temperature range 273 to 823 K:

$$\Delta E^f_{\alpha \to \delta}(T) = 3 \times 10^{-10}T^3 - 2 \times 10^{-7}T^2 + 4 \times 10^{-4}T - 0.5655 \left[\dfrac{eV}{at}\right] \quad (14)$$

Growth: Growth can be controlled either by the diffusion of hydrogen (i.e., by the time required for hydrogen to travel in zirconium and find a hydride nucleus) or by the surface reaction (i.e., by the time needed for hydrogen in solid solution to react with the zirconium matrix to form more of the hydride phase). Both reactions have their own kinetic constant, that is, their own K_G parameter. In a diffusion-controlled process, the constant is noted as K^D_G as shown in figure 4. The Avrami parameter found when fitting the different values of K_G was $p = 2.56$ (as shown in the earlier section on isothermal growth measured using DSC). The value used for the Avrami parameter is 2.5, which in the JMAK model corresponds to platelet-shaped particles, in agreement with experiments.[23,24,36,37] The activation energy for the reaction-driven growth kinetics parameter K^R_G is taken to be the same activation energy for the nucleation process because the process is controlled by the formation of new hydride material. The pre-exponential factor was fitted to match the point at 320°C for Sample C in figure 3, using the activation energy defined in equation (14): $E(320°C) = -0.336\ eV/atom$. The pre-exponential factors for K^R_G and K^D_G were assumed to be linearly dependent on hydrogen concentration and linearly dependent on the remaining volume fraction of zirconium. As a result, the two values of K^R_G and K^D_G (expressed in s^{-1}) are given by equations (15) and (16), respectively:

$$\text{Diffusion-controlled}: K^R_G = 5.53 \times 10^5 \cdot v_0 \cdot f_\alpha \cdot \exp -\dfrac{0.9}{k_B T} \quad [s^{-1}] \quad (15)$$

$$\text{Reaction-controlled}: K^R_G = 1.6 \times 10^{-5} \cdot v_0 \cdot f_\alpha \cdot \exp -\dfrac{\Delta E^f_{\alpha \to \delta}}{k_B T} \quad [s^{-1}] \quad (16)$$

where ν_0 is defined using the phase diagram lever rule by $\nu_0 = \frac{x_0 - x_\alpha}{x_\delta - x_\alpha}$ where x_0 is the total hydrogen atomic fraction, x_α the atomic fraction of hydrogen in the α phase at the $\alpha/(\alpha + \delta)$ boundary of the Zr-H phase diagram, and x_δ the atomic fraction in the hydride at the $(\alpha + \delta)/\delta$ boundary of the phase diagram; x_δ can be found for every temperature by solving equation (13) for different temperatures; and x_δ can be fitted to a third-degree polynomial, as shown in equation (17):

$$x_\delta(T) = -9.93 \times 10^{-11} T^3 + 8.48 \times 10^{-8} T^2 - 5.73 \times 10^{-5} T + 0.6238 \qquad (17)$$

where T is expressed in Kelvin; $x_\alpha(T)$ is obtained by converting the value of TSS_D chosen for the model from wt.ppm to atomic percent.

The value of K_G reflects the slowest process as the rate limiting step, according to equation (18):

$$\frac{1}{K_G} = \frac{1}{K_G^D} + \frac{1}{K_G^R} \qquad (18)$$

Note that a dependence of hydride growth on either δ-hydride phase content or α-zirconium has not been observed. However, a linear dependence has been implemented as a first approximation to reflect work that has been performed previously where a linear dependence on the volume fraction of α-zirconium was implemented to avoid precipitation over the maximum amount of hydrogen that can be accommodated by the hydride phase.[13] This dependence does not significantly impact model predictions at low hydrogen content (< 500 wt.ppm) because $f_\alpha > 0.9$ in that range. In parallel, hydride growth is hypothesized to be dependent on the volume fraction of hydrides present because the more hydrides there are the easier it is for a hydrogen atom in supersolubility to find a hydride particle on which to grow more of the preexisting hydride phase.

Dissolution: The dissolution parameter used in the model is given by equation (19):

$$K_D = 4.11 \times 10^3 \cdot \exp -\frac{E_D}{K_B T} \quad [s^{-1}] \qquad (19)$$

While the results in figure 8 suggest that the dissolution kinetics parameter decreases at high temperature, it is yet unclear why this is the case.

PRELIMINARY BENCHMARK OF THE MODEL

It is important to benchmark the model to ensure that its predictions correspond to experimental observation. In this study, a benchmark was performed to ensure that hydride precipitation and dissolution kinetics correspond to experimental observations. The cyclic hydride precipitation and dissolution of a sample containing 255 wt.ppm of hydrogen[15] was simulated. The HNGD predictions were compared to the results of the model in the three-dimensional finite element fuel performance code BISON[13] and to experimental data.[15] Figure 9 shows the concentration of hydrogen in solid solution when a sample is subjected to the temperature schedule shown by the red dotted line. The HNGD model results presented used TSS_D and

FIG. 9 Hydrogen concentration in solid solution as a function of time for the temperature schedule shown (dashed and dotted line), including the simulation of the experiment performed[15] (sample containing 255 wt.ppm of hydrogen) with two different models: the HNGD model (dashed line) but with *TSS* values derived from the first heat up and cool down cycle (t ≤ 4,000 s) and the model presented by Courty et al.[10] and used in BISON,[13] with the same values of TSS_D and TSS_P. The model currently used in BISON (dotted line) fails to accurately predict hydride precipitation, whereas the HNGD model provides a better prediction of the hydrogen content in solid solution.
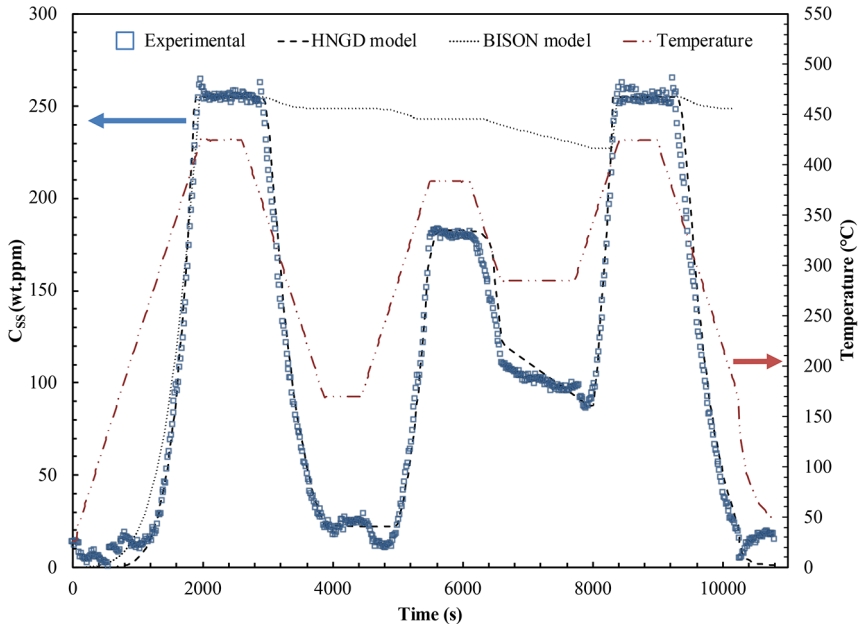
TSS_P interpolated from the hydrogen content in solid solution measured experimentally during the first ramp-up and ramp-down cycle.

As can be observed, the HNGD model is more accurate than the previously used BISON model. This is primarily because the BISON model relies solely on diffusion experiments performed by Kammenzind et al.[12] to measure hydride precipitation kinetics for the model.[31] Because diffusion is a slow process, it is not surprising that it is not representative of mechanisms involved in transient conditions such as simulated here. In the HNGD model, hydride precipitation occurs by nucleation when the hydrogen content in solid solution is above TSS_P. This is much faster than precipitation during isothermal holds or diffusion experiments and causes the hydrogen content in solid solution to decrease rapidly in a similar fashion as observed experimentally. **Figure 9** shows that modeling the precipitation of

hydrogen using this hypothesis yields better results in "transient" conditions than the model implemented in BISON.

The model currently accounts for the influence of temperature, hydrogen in solid solution, as well as hydride and zirconium volume fraction on the precipitation rate of zirconium hydrides in zirconium. In another paper in preparation, the HNGD model, which is being implemented in BISON, is verified and validated for a given range of hydrogen contents and cooling rates on a wider set of experimental data.

Conclusions

A series of experiments was performed to study hydride precipitation and dissolution in Zircaloy-4. The principal results are:

- Precipitation of hydrogen during isothermal hold occurs until the hydrogen in solid solution reaches TSS_D. This can be quantified using DSC. It is possible to distinguish between hydride nucleation and hydride growth by examining different aspects of the diffraction and DSC data.
- A significant increase in TSS_P was observed during hydride precipitation upon cooling from high temperature when an applied stress was present that was high enough to cause hydride reorientation, indicating that the precipitation of reoriented hydrides occurs at a greater undercooling than that of in-plane hydrides. In contrast, applied stress did not significantly affect hydride precipitation kinetics.
- No significant effect of applied stress was observed on hydride dissolution upon heating in the temperature range of 150 to 380°C.

The analysis of the previous experimental data was used to develop the HNGD model, which can describe hydride precipitation in all regimes (including the hysteresis region).

- The HNGD model predicts that hydrides continue to precipitate during an isothermal hold, in agreement with experimental observations, and predicts hydride dissolution if hydrogen in solid solution is lower than TSS_D when hydrides are present.
- The HNGD model can provide an estimate of the specific fractions of hydrogen precipitation that occur by hydride nucleation and by hydride growth.

preparation and in running the DSC. Use of the APS was supported by the U.S. Department of Energy, Office of Basic Energy Sciences, under Contract No. DE-AC02-06CH11357.

References

1. A. T. Motta, A. Couet, and R. J. Comstock, "Corrosion of Zirconium Alloys Used for Nuclear Fuel Cladding," *Annual Review of Materials Research* 45 (2015): 311–343.

2. A. Couet, A. T. Motta, R. J. Comstock, and A. Ambard, "Oxide Electronic Conductivity and Hydrogen Fraction in Zr Alloys," in *Transactions of the American Nuclear Society and Embedded Topical Meeting: Nuclear Fuels and Structural Materials for the Next Generation Nuclear Reactors* 110 (2014): 845–848.

3. N. Ramasubramanian, "Localised Electron Transport in Corroding Zirconium Alloys," *Journal of Nuclear Materials* 55 (1975): 134–154.

4. K. Une and S. Ishimoto, "Dissolution and Precipitation Behavior of Hydrides in Zircaloy-2 and High Fe Zircaloy," *Journal of Nuclear Materials* 322 (2003): 66–72.

5. A. McMinn, E. C. Darby, and J. S. Schofield, "The Terminal Solid Solubility of Hydrogen in Zirconium Alloys," in *Zirconium in the Nuclear Industry: Twelfth International Symposium,* ed. G. Sabol and G. Moan (West Conshohocken, PA: ASTM International, 2000), 173–195, https://doi.org/10.1520/STP14300S

6. K. Colas, A. T. Motta, M. R. Daymond, and J. D. Almer, "Mechanisms of Hydride Reorientation in Zircaloy-4 Studied In Situ," in *Zirconium in the Nuclear Industry: 17th Internation Symposium,* ed. B. Comstock and P. Barberis (West Conshohocken, PA: ASTM International, 2014), 1107–1137, https://doi.org/10.1520/STP154320120168

7. G. F. Slattery, "The Terminal Solubility of Hydrogen in the Zirconium/2 at % Chromium/0.16 at % Iron Alloy," *Journal of Nuclear Materials* 32 (1969): 30–38.

8. R. Tang and X. Yang, "Dissolution and Precipitation Behaviors of Hydrides in N18, Zry-4 and M5 Alloys," *International Journal of Hydrogen Energy* 34 (2009): 7269–7274.

9. P. Vizcaino, A. V. Flores, P. B. Bozzano, A. D. Banchik, R. A. Versaci, and R. O. Rios, "Hydrogen Solubility and Microstructural Changes in Zircaloy-4 Due to Neutron Irradiation," *Journal of ASTM International* 8 (2011): 1–20.

10. O. Courty, A. T. Motta, and J. D. Hales, "Modeling and Simulation of Hydrogen Behavior in Zircaloy-4 Fuel Cladding," *Journal of Nuclear Materials* 452 (2014): 311–329.

11. O. Courty, A. T. Motta, C. J. Piotrowski, and J. D. Almer, "Hydride Precipitation Kinetics in Zircaloy-4 Studied Using Synchrotron X-Ray Diffraction," *Journal of Nuclear Materials* 461 (2015): 180–185.

12. B. F. Kammenzind, D. G. Franklin, H. R. Peters, and W. J. Duffin, "Hydrogen Pickup and Redistribution in Alpha-Annealed Zircaloy-4," in *Zirconium in the Nuclear Industry: Eleventh International Symposium,* ed. E. Bradley and G. Sabol (West Conshohocken, PA: ASTM International, 1996), 338–370, https://doi.org/10.1520/STP16180S

13. D. S. Stafford, "Multidimensional Simulations of Hydrides during Fuel Rod Lifecycle," *Journal of Nuclear Materials* 466 (2015): 362–372.

14. E. Lacroix and A. T. Motta, "Validation of BISON Calculation of Hydrogen Distribution by Comparison to Experiment," in *TMS 2016: 145th Annual Meeting & Exhibition* (Cham, Switzerland: Springer, 2016), 263–272.

15. E. Lacroix, A. T. Motta, and J. D. Almer, "Experimental Determination of Zirconium Hydride Precipitation and Dissolution in Zirconium Alloy," *Journal of Nuclear Materials* 509 (2018): 162–167.

16.   O. Zanellato, K. Preuss, J.-Y. Buffiere, F. Ribeiro, A. Steuwer, J. Desquines, J. Andrieux, and B. Kerbs, "Synchrotron Diffraction Study of Dissolution and Precipitation Kinetics of Hydrides in Zircaloy-4," *Journal of Nuclear Materials* 420, nos. 1–3 (2012): 537–547.

17.   J. W. Mullin, *Crystallization*, 4th ed. (Oxford, UK: Butterworth Heinemann, 2001).

18.   P. Raynaud, D. A. Koss, A. T. Motta, and K. S. Chan, "Fracture Toughness of Hydrided Zircaloy-4 Sheet under Through-Thickness Crack Growth Conditions," in *Zirconium in the Nuclear Industry: 15th Internathinal Symposium*, ed. B. Kammenzind and M. Limbäck (West Conshohocken, PA: ASTM International, 2007), 163–177, https://doi.org/10.1520/STP48135S

19.   E. Tenckhoff, "Review of Deformation Mechanisms, Texture, and Mechanical Anisotropy in Zirconium and Zirconium Base Alloys," *Journal of ASTM International* 2, no. 4 (2005): 1–26, https://doi.org/10.1520/JAI12945

20.   J. J. Kearns and C. R. Woods, "Effect of Texture, Grain Size, and Cold Work on the Precipitation of Oriented Hydrides in Zircaloy Tubing and Plate," *Journal of Nuclear Materials* 20 (1966): 241–261.

21.   P. Delobelle, P. Robinet, P. Bouffioux, P. Geyer, and I. Le Pichon, "A Unified Model to Describe the Anisotropic Viscoplastic Behavior of Zircaloy-4 Cladding Tubes," in *Zirconium in the Nuclear Industry: 11th International Symposium,* ed. E. Bradley and G. Sabol (West Conshohocken, PA: ASTM International, 1996), 373–393, https://doi.org/10.1520/STP16181S

22.   *Standard Test Method for Kinetic Parameters by Differential Scanning Calorimetry Using Isothermal Methods,* ASTM E2070-13 (West Conshocken, PA: ASTM International, approved September 15, 2013).

23.   A. T. W. Barrow, A. Korinek, and M. R. Daymond, "Evaluating Zirconium-Zirconium Hydride Interfacial Strains by Nano-Beam Electron Diffraction," *Journal of Nuclear Materials* 432 (2013): 366–370.

24.   M. N. Cinbiz, D. A. Koss, and A. T. Motta, "The Influence of Stress State on the Reorientation of Hydrides in a Zirconium Alloy," *Journal of Nuclear Materials* 477 (2016): 157–164.

25.   M. N. Cinbiz, D. A. Koss, A. T. Motta, J. S. Park, and J. D. Almer, "In Situ Synchrotron X-Ray Diffraction Study of Hydrides in Zircaloy-4 during Thermomechanical Cycling," *Journal of Nuclear Materials* 487 (2017): 247–259.

26.   M. Avrami, "Kinetics of Phase Change. I: General Theory," *The Journal of Chemical Physics* 7 (1939): 1103–1112.

27.   M. Avrami, "Kinetics of Phase Change. II Transformation-Time Relations for Random Distribution of Nuclei," *The Journal of Chemical Physics* 8 (1940): 212–224.

28.   M. Avrami, "Granulation, Phase Change, and Microstructure Kinetics of Phase Change. III," *The Journal of Chemical Physics* 9 (1941): 177–184.

29.   J. J. Kearns, "Diffusion Coefficient of Hydrogen in Alpha Zirconium Zircaloy-2 and Zircaloy-4," *Journal of Nuclear Materials* 43 (1972): 330–338.

30.   Y. Zhang, C. Jiang, and X. Bai, "Anisotropic Hydrogen Diffusion in α-Zr and Zircaloy Predicted by Accelerated Kinetic Monte Carlo Simulations," *Scientific Reports* 7 (2017): 1–13.

31.   G. P. Marino, "Hydrogen Supercharging in Zircaloy," *Materials Science and Engineering* 7 (1971): 335–341.

32.   C. Domain, R. Besson, and A. Legris, "Atomic-Scale Ab-Initio Study of the Zr-H System: I. Bulk Properties," *Acta Materialia* 50 (2002): 3513–3526.

33.   J. J. Kearns, "Dissolution Kinetics of Hydride Platelets in Zircaloy-4," *Journal of Nuclear Materials* 27 (1968): 64–72.

34.   N. Dupin, I. Ansara, C. Servant, C. Toffolon, C. Lemaignan, and J. C. Brachet, "A Thermodynamic Database for Zirconium Alloys," *Journal of Nuclear Materials* 275 (1999): 287–295.

35. A. M. Jokisaari and K. Thornton, "General Method for Incorporating CALPHAD Free Energies of Mixing into Phase Field Models: Application to the α-Zirconium/δ-Hydride System," *Calphad* 51 (2015): 334–343.

36. N. A. P. K. Kumar, J. A. Szpunar, and Z. He, "Preferential Precipitation of Hydrides in Textured Zircaloy-4 Sheets," *Journal of Nuclear Materials* 403 (2010): 101–107.

37. N. A. P. K. Kumar and J. A. Szpunar, "EBSD Studies on Microstructure and Crystallographic Orientation of δ-Hydrides in Zircaloy-4, Zr-1% Nb and Zr-2.5% Nb," *Journal of Nuclear Materials* 528 (2011): 6366–6374.

38. E. Lacroix, "Modeling Zirconium Hydride Precipitation and Dissolution in Zirconium Alloys" (PhD dissertation, The Pennsylvania State University, 2019).

Discussion

Question from Mirco Grosse, KIT:—The penetration depth of an X-ray is usually a couple of microns. Are there hints that the results obtained at the surface of the sample can be extrapolated to the bulk of the material?

Authors' Response:—The X-ray source used in this study is a high-energy X-ray synchrotron source from Argonne National Laboratory's APS. The energy used was 71.676 keV, which allowed the X-rays to traverse the entire thickness of our 660-μm-thick sample. The measurements are thus over the entire thickness of the sample and are, therefore, representative of the bulk of the material.

Question from Sean Hanlon, CNL:—On cooling (e.g., at 1°C/min), do you assume nucleation is dominant, while during a hold, growth is dominant? Does this suggest hydrides will have a significantly smaller average size if they form during cooling versus during a hold?

Authors' Response:—Although the cooling rate dictates what precipitation mechanism dominates, the differences may not be as stark among hydride morphologies, so that a hydride precipitated during cooling at a 1°C/min rate may be relatively similar to a hydride precipitated during a long isothermal hold.

However, at higher cooling rates, the effect may be more pronounced. For reference, the primary author has published in his dissertation[38] a detailed comparison of hydride lengths formed in two sister samples: one cooled from 450°C at a rate of 15°C/min and another, cooled at 15°C/min to 300°C, held at 300°C for 5 h, and then cooled to room temperature at 15°C/min. The study was made over a population greater than 750 hydrides. The average hydride size in the first was 1.78 μm ± 0.82 μm compared to an average size of 2.35 μm ± 2.12 μm in the second.

Questions from Nima Nikpoor Badr, Queen's University:
1. Did you observe any effect of T_{max} on TSS_p?
2. In recent literature, it is shown that after nucleation starts during cooling, in the first 50°C range of precipitation, γ-hydride forms and then it transforms to δ-hydride at lower temperatures. Did you observe this phenomenon?

Authors' Response:
1. We do not know. So as to exclude any possible effect of the maximum temperature on the supersolubility limit, all precipitation studies were made with the same maximum temperature: $T_{max} = 400°C$ (with the exception of Sample D described in the paper, which was not used to fit the model but only to verify it).
2. The gamma hydride peaks are quite distinct from the delta peaks and, in the experiments conducted not only in this study but previous others from our group, no gamma peaks were seen. The peaks detected and indexed corresponded only to δ-hydrides from the beginning of the precipitation to the end. The phenomenon mentioned was therefore not observed.

Question from Antoine Ambard, EDF:—To measure the TTT diagram, you use DSC. The reaction rate is low, and the hydride fraction precipitating is low. Could you comment on the error or uncertainty entering these measurements?

Authors' Response:—Although the reaction rate and hydride fraction are low and the signal obtained is low, it is detectable. We evaluate that if the reaction time is underpredicted or overpredicted by 10 min, the associated uncertainty in evaluating the time for the reaction to finish is lower than 5%.

The biggest contributor to the uncertainty in calculating the advancement of the reaction is the values taken for TSS_P and TSS_D at the hold temperature and the measurement on the hydrogen content in the sample. As seen in the literature, TSS_P measurements can vary significantly, and we believe this is the primary source of uncertainty in the model.

However, the model predicts the behavior of a sample, independent of the data used to fit the model accurately (fig. 9), suggesting that the parameters chosen for the presented model are at least reasonably accurate. However, the HNGD model is a new model, with only limited data available to fit it. Additional studies could quantify these uncertainties and the effect of other factors (the cooling rate, for example) on the fitted parameters.

Question from Bruce Kammenzind, Naval Nuclear Labs:—You mentioned that you put a hydride dependence upon the rate parameters. Can you comment on whether the rate dependencies will increase or decrease kinetics as a function of hydride volume fraction?

Authors' Response:—It is expected that increasing the hydride volume fraction will increase the growth kinetics as an increased surface area density is available for hydride growth. From this perspective, it would also mean that a higher cooling rate would lead to an increase in growth kinetics as the hydride surface density increases for small hydrides due to their higher surface to volume ratio, which favors hydride growth. This hypothesis, however, needs to be tested.

Question from Clara Anghel, Westinghouse Electric Sweden:—In your experiments, was all the hydrogen in solution before cooling? There are previous investigations that show that the presence of hydrides before (i.e., hydrogen content above solubility limit) will have an impact on the nucleation of new hydrides. During cooling, in this case, hydrogen will diffuse preferentially toward the existing hydrides, and the existing hydrides will grow in favor of nucleating new hydrides. The growth versus nucleation changes in this case. Have you considered this process in your model?

Authors' Response:—Yes, all the hydrides were dissolved, and only hydrogen in solid solution was present. This was ensured by observing the disappearance of the brightest peak by diffraction and by observing the typical dissolution peak in DSC.

The HNGD model considers the process mentioned and can reproduce this phenomenon, as observed in figure 9, where the HNGD prediction is compared to the results of one of the studies that highlights the phenomenon you describe (see Lacroix, Motta, and Almer[15] in the paper). We do agree that preexisting hydrides will affect (increase) nucleation of new hydrides. However, we believe that the dominant form of precipitation comes from growth of preexisting hydrides rather than nucleation of new hydrides.

Question from Ted Darby, Rolls-Royce:—Have you considered the implications of your observations and model (based on kinetic effects in the bulk) to hydride behavior at a local crack tip? Is there an inference that DHC would not be sustained under isothermal conditions?

Authors' Response:—The model described here is only the phenomenon of precipitation and dissolution in the absence of stress or a stress gradient. The results presented here are, therefore, not representative of DHC conditions, so we have not considered the implications of the current work to that phenomenon.

Question from Mark Wenman, Imperial College London:—What alloy was used? And have you considered using different tin (Sn) contents as it should shift your TTT curve?

Authors' Response:—Cold-worked stress-relieved Zircaloy-4 was used. The primary goal of this project was to better understand the precipitation kinetics of hydrides and the role of the "hysteresis" in the precipitation kinetics.

Although the hydride precipitation behavior may change in other alloys because of microstructure or chemical effects, this was not studied in the present work.